

Fractional derivative and hereditary combined model for memory effects on flexible polyurethane foam

Makram Elfarhani¹ · Abdessalem Jarraya¹ ·
Said Abid¹ · Mohamed Haddar¹

Received: 12 August 2015 / Accepted: 7 January 2016 / Published online: 27 January 2016
© Springer Science+Business Media Dordrecht 2016

Abstract In a quasi-static regime with cyclic loading, the force–displacement curve of flexible polyurethane exhibits complicated behavior: nonlinearity, visco-elasticity, hysteresis, residual force, etc. Beside nonlinearity and visco-elasticity, this material displays high dependence on the displacement rate and past loading history. Its dependence on compression rate helps to appropriately identify the force–displacement curve. Based on the new curve identification, the overall foam response is assumed to be a composite of a nonlinear elastic component and a visco-elastic component. The elastic component is expressed as a polynomial function in displacement, while the visco-elastic one is formulated according to the hereditary approach to represent the foam visco-elastic damping force during the loading phase and according to the fractional derivative approach during unloading to represent the visco-elastic residual force in the material. The focus of this study was to develop mathematical formulations and identification parameters to faithfully characterize the visco-elastic behavior of flexible polyurethane foam under multi-cycle compressive tests. A parameter calibration methodology based on the separation of the measurement data of each component force was established. This optimization process helps to avoid the parameter values admixture problem during the phase of numeric calculations of the same component force. The validity of the model results is checked according to the simulation accuracy, the physical significance of results and their agreement with the obtained force–displacement curve identification.

Keywords Flexible polyurethane foam · Quasi-static behavior · Multiple cycle compression test · Visco-elasticity · Memory effects · Fractional derivative approach · Hereditary approach

Nomenclature

x Displacement [mm]
 \dot{x} Displacement rate [mm s^{-1}]

✉ M. Elfarhani
makram.farhani@gmail.com

¹ Mechanics, Modeling and Production Laboratory (LA2MP), National Engineering School of Sfax (ENIS), B.P.W. 3038, Sfax, Tunisia

t	Time [s]
T	Total testing duration [s]
A	Maximum displacement level [mm]
F_L	Total foam response during loading half-cycle [N]
F_U	Total foam response during unloading half-cycle [N]
E_L	Nonlinear elastic force during loading half-cycle [N]
E_U	Nonlinear elastic force during unloading half-cycle [N]
V_D	Visco-elastic damping component [N]
V_R	Visco-elastic residual force component [N]
Q	Objective function [N ²]
a_i	Visco-elastic damping coefficient of order i [N mm ⁻¹ s ⁻¹]
α_i	Visco-elastic damping parameter [Hz]
k_i	Elastic stiffness of order i [N mm ⁻¹]
r_i	Visco-elastic residual force coefficient of order i [N s ^{β} m ⁻¹]
δx	Displacement sampling [mm]
β_i	Fractional order
Γ	Gamma function
M	Order of fractional derivative terms
N	Order of the visco-elastic kernel
P	Order of elastic polynomial function
S	Sampling number

1 Introduction

Flexible polyurethane foam is an important visco-elastic material widely used in various engineering applications (Gibson and Ashby 1997). It has special mechanical characteristics such as low density, high energy absorption capacity, low stiffness, and many others. These prominent properties still stimulate car manufacturers to use soft polyurethane foam as a major element in modern automotive seats. However, many of its mechanical behavioral aspects are not yet completely understood. Beside nonlinearity and visco-elasticity, soft foam displays a memory of past loading history and requires sufficient time to recover. To characterize this complex mechanical behavior, a multi-cycle uniaxial compression test in a quasi-static regime was considered in this study. This standard involves imposing three consecutive cycles on a soft foam sample, each including a compression phase and decompression one. The objectives of this test are to investigate the changes in foam response with repetitive loading and to unveil an important part of the material's behavioral potential (Puri 2004).

Among several analyses used in visco-elastic and cellular materials literature, the macroscopic analysis is particularly promising since it has yielded experimental and analytical interpretations. It is based on the assumption that the foam specimen size is much greater than that of the micro-structural units (cells) and that the behavior of foam is studied as a continuum. Through this analysis, this work considered two main memory formulations: the hereditary and the fractional derivative models. Both are derived from the differential form models, where constitutive laws are given as a time differential equation of integer orders (case of hereditary formulation, Ferry 1970) or of non-integer orders (case of fractional derivative formulation, Bagley and Torvik 1983). The application of the Boltzmann superposition principle in the integer order differential form models leads to the convolution form models that include an integral term with a relaxation kernel. Del Piero and Pampolini

(2012) proposed a rheological representation of the response of open-cell polymeric foams and used the convolution formulation to model its dissipative elements. This model leads to good numerical simulations for a series of experiments including the cyclic compression tests. In hereditary models, the stress is assumed to be a convolution form of strain history weighing by the relaxation kernel (Christensen 1982). Yu and Haddad (1994) showed that the relaxation kernel is better defined as a sum of exponentials. Ippili et al. (2003) and White et al. (2000) used a hereditary model with an exponential kernel to depict the visco-elastic behavior of polyurethane foam in quasi-static and dynamic regimes, respectively. Jmal et al. (2011) produced accurate predictions using this model for three types of polyurethane foam.

The fractional derivative approach is also widely used to characterize memory effects in visco-elastic materials since it has theoretical and experimental reasons. In studies by Nutting (1921), relaxation effects were found to be expressed by fractional powers of time, and the stress–strain relationship in the molecular theory of Rouse (1953) was expressed in fractional derivative terms. Deng et al. (2006) obtained accurate predictions of polyurethane foam response undergoing multi-cycle compressive tests with a five-parameter fractional derivative model. The aim of this paper is to develop mathematical formulations to faithfully characterize the visco-elastic behavior of flexible polyurethane foam under uniaxial cyclic compression tests in a quasi-static regime. The model formulations consider hereditary and fractional derivative approaches. Each formulation is applied in its appropriate testing phase according to a new interpretation of the force–displacement. An identification methodology of parameters is developed based on separation of the measurement data of the elastic and visco-elastic parts of the total foam response. The fitting accuracy and the model's potential to yield good and reasonable simulations are discussed.

2 Force–displacement curve of flexible polyurethane foam

2.1 Experimental setup

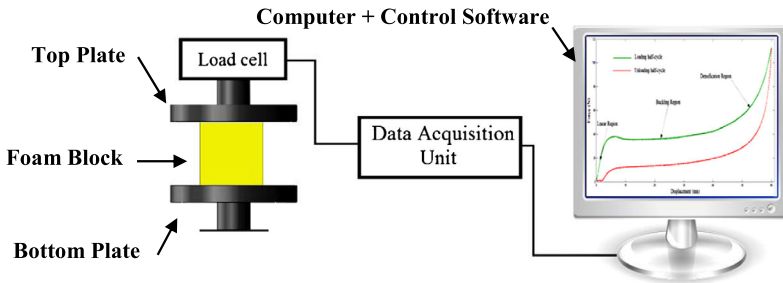
To study foam visco-elastic behavior in a quasi-static regime, uniaxial compressive tests were conducted on polyurethane foam open cell samples obtained by cutting a virgin mattress in cubic blocks. The mean properties of the material specimens are shown in Table 1.

The experimental setup representation for compression tests on foam specimens is shown in Fig. 1. Experiments were executed in a universal testing machine useful for uniaxial loading tests. During a single compression test, the foam sample was placed between two parallel plates. The bottom plate which supports the material specimen was kept fixed, while the top plate which is related to the load cell was programmed to displace down up to 80 % of the foam initial height, and returned to zero position at the same cross-head speed. The sampling rate was set to 16 s^{-1} .

The material response and the compression displacement were measured by using, respectively, a load cell that had a 500 N capacity and a displacement sensor. The testing machine provided a displacement resolution of 0.001 mm, and an accuracy of the testing force less than 0.5 % of indicative value, and it had a speed range between 0.005 to 500 mm/min. Once the first cycle of compression was completed, we observed a residual strain in the foam sample, and contact between the top plate and the material was lost. For multiple compression cycles, the upper plate was programmed to rerun the loading and the unloading paths after reaching the zero position. In this experimental study, three consecutive cycles were considered.

Table 1 Characteristics of tested foam samples

Foam type	Flexible polyurethane foam
Designation	Type A
Cell type	Open
Density	28 kg/m ³
Porosity	95 %
Pores size	200–250 μm
Specimen shape	Cubic
Initial dimensions (L_0)	75 mm

**Fig. 1** Experimental setup of uniaxial compressive tests

2.2 Force–displacement curve of multiple consecutive cycles

In this investigation, we assumed a zero Poisson's ratio for the material specimen. This assumption is based on experimental observations of the tested foam specimen where it was found that the material has a Poisson's ratio very near to zero at 80 % compressions. Furthermore, this hypothesis is adopted in several investigations including the study by Mills and Gilchrist (2000), and Deng et al. (2004, 2006). As known, force–displacement curves of flexible foam undergoing a cyclic loading include two visco-elastic manifestations: the hysteretic and the memory effects. In Fig. 2, we show the typical response of a polyurethane foam sample subjected to three consecutive cycles. The green lines denote the loading paths and the red ones the unloading paths. In the cellular solids literature, the complex behavior of soft polyurethane foam is assigned to visco-elasticity of polymer solid and to the matrix structure of the material as well. According to the micro-mechanical analysis, Gibson and Ashby (1997) suggested an identification of the loading part of the foam force–displacement curve according to the deformation mechanisms that the material microstructure units (cells) undergo. Through this identification, the curve can be subdivided into three compression regions: linear, buckling, and densification. Each corresponds to a specific compression mechanism of cells struts.

In this paper, we propose a new identification of the force–displacement curve based on experimental observations of visco-elastic manifestations in the macro-level behavior of polyurethane foam.

2.3 Phenomenological identification of the force–displacement curve

According to several authors (Bagley and Torvik 1983; Singh 2000; Ippili et al. 2003; Del Piero and Pampolini 2012), the total foam response to uniaxial compression is assumed to

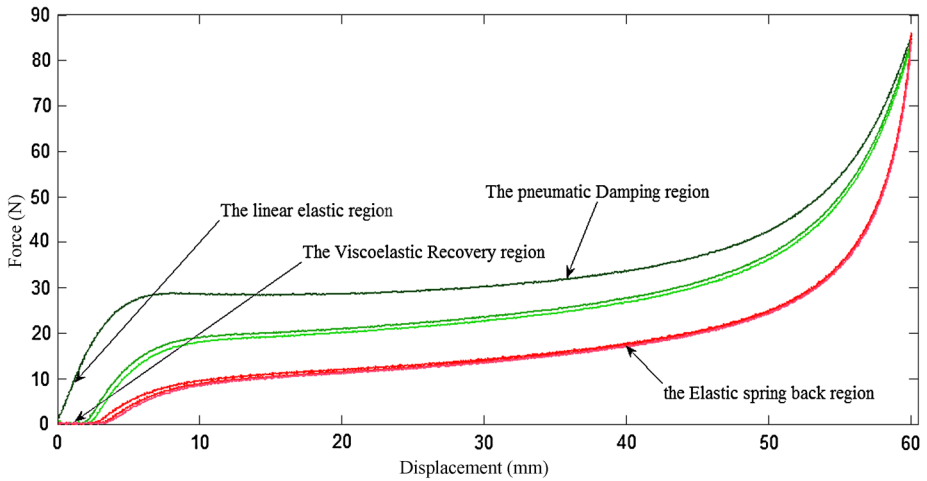


Fig. 2 Typical response of polyurethane foam after three consecutive cycles

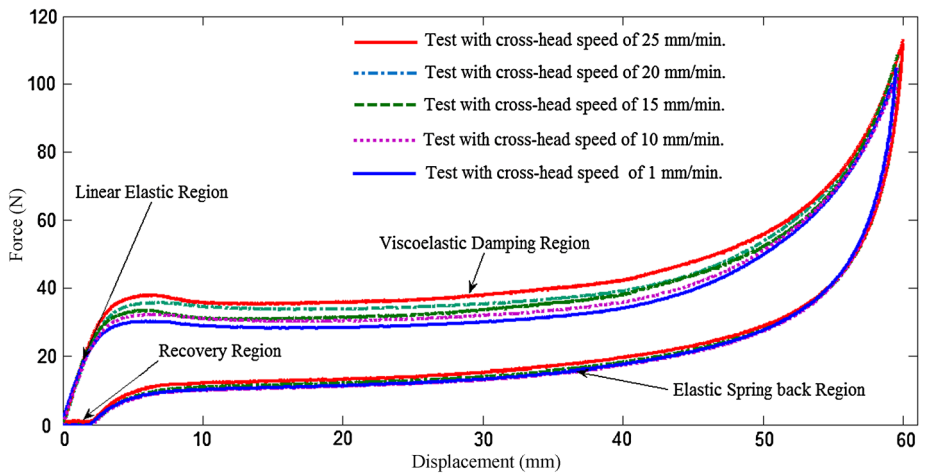


Fig. 3 Compressive force–displacement curves obtained with different cross-head speeds

be a sum of a linear visco-elastic component and a nonlinear elastic component. However, most of the behavioral characteristics of these components are not completely understood. It is commonly known that the visco-elastic force which, contrary to the elastic force, is affected by the variation of the displacement rates. Therefore, comparing the shapes and the magnitudes of different parts of force–displacement curves produced by different time durations tests helps to clearly identify the regions where each component lies. In Fig. 3, we plotted the experimental results of uniaxial compressive tests performed with different loading cross-head speeds. Each plot represents the mean curve of test results executed on four foam specimens. According to Gauch (2006), four repeats of each test guarantee a 70.5 % probability that the mean curves are reproducible.

From Fig. 3, we observe that all curves have almost the same shape. Yet, some parts of the curves show a significantly high dependence on the loading cross-head speed, while it is

completely or partially absent in others. Hence, we identify four regions in the loading and unloading curves: (i) linear elastic, (ii) visco-elastic damping, (iii) elastic spring back, and (iv) recovery.

The linear elastic region does not at all depend on the loading cross-head speed which makes the foam response completely elastic. This is because the air contained within the cells remains motionless. This region fades starting from the second cycle in multi-cycle tests. The visco-elastic damping region is highly dependent on the displacement rate. The higher the displacement rate, the more elevated the material response magnitude. Hence, the visco-elastic component exists in this region with the elastic one. Here, the dependence on the loading cross-head speed is linked to the damping of the foam by the air exhaust through the material pores.

The displacement rate is not very important to the elastic spring back region. The elastic return does not change noticeably in all loading cross-head speeds. Here, the weak dependence is caused by the residual strain at the loading phase. This phenomenon shows the visco-elasticity of the polyurethane matrix.

In the recovery region, the machine top plate loses contact with the foam sample. Thus, the material response is entirely absent. Here, the material takes many hours, or even days, to recuperate its initial dimensions. Since the response is not instantaneous and residual effects keep decreasing with time, the recovery region seems to have only a purely visco-elastic component.

Figure 3 shows that the four regions are clear-cut in the monocycle's curve. However, the linear elastic and the recovery regions appear only in the first cycle and fade in the subsequent cycles of a multi-cycle test.

In the next section, the formulations of the model that refer to this new curve identification are established to characterize the visco-elastic behavior of polyurethane foam.

3 Modeling the foam response under multiple-cycle tests

According to the curve identification described above, the elastic component is present in all cycles and during both the loading and the unloading phases since it does not depend either on the displacement rate or the number of cycles; while the visco-elastic component is manifested during the loading phase of the first cycle by a visco-elastic damping component and during the unloading phase by a visco-elastic residual force component. Hence, the total force exerted by the foam specimen during the loading and the unloading phases of the first cycle is respectively expressed as:

$$F_{L1}(x(t)) = E_{L1}(x(t)) + V_{D1}(x(t)), \quad (1)$$

$$F_{U1}(x(t)) = E_{U1}(x(t)) + V_{R1}(x(t)). \quad (2)$$

E_{L1} and E_{U1} are the elastic components whereas V_{D1} and V_{R1} are the visco-elastic components.

For subsequent cycles, the foam block is obviously not fully recovered. Thus the visco-elastic residual force component exists in the total foam response during the unloading as well as the loading phases for the second and third cycles. Hence, the total foam response during both phases of the second cycle is respectively expressed as:

$$F_{L2}(x(t)) = E_{L2}(x(t)) + V_{D2}(x(t)) + V_{R1}(x(t)), \quad (3)$$

$$F_{U2}(x(t)) = E_{U2}(x(t)) + V_{R1}(x(t)) + V_{R2}(x(t)). \quad (4)$$

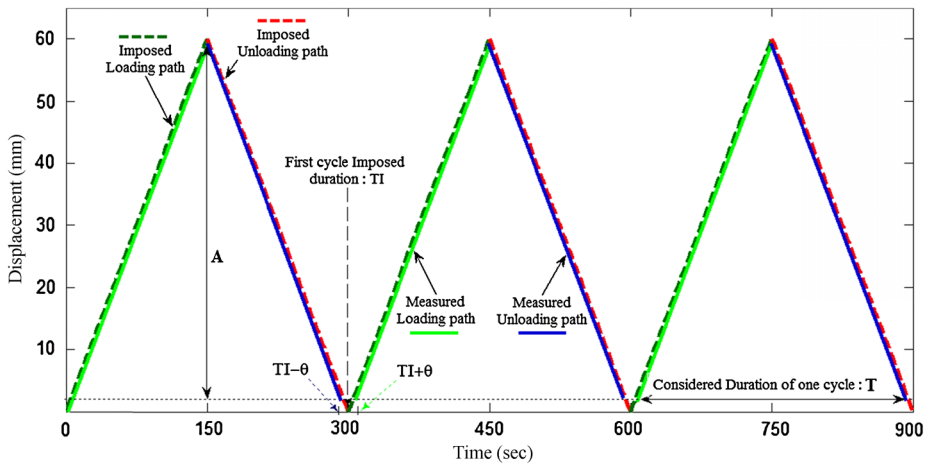


Fig. 4 Imposed and measured displacement of cyclic compressive uniaxial test

In the same way, the visco-elastic residual force component of the second cycle exists in the total foam response of the third loading phase. Thus, its expression is given as:

$$F_{L3}(x(t)) = E_{L3}(x(t)) + V_{D3}(x(t)) + V_{R1}(x(t)) + V_{R2}(x(t)), \tag{5}$$

$$F_{U3}(x(t)) = E_{U3}(x(t)) + V_{R1}(x(t)) + V_{R2}(x(t)) + V_{R3}(x(t)). \tag{6}$$

With reference to phenomenological identification of the force–displacement curve, visco-elasticity is manifested by various aspects and origins. Hence, the visco-elastic components during loading and unloading must be modeled using different visco-elastic approaches, and then different mathematical formulations.

3.1 Displacement expressions

For a quasi-static and multi-cycle compression test with a constant loading cross-head speed, the displacement $x(t)$ is a linear function of time in each half cycle. Figure 4 shows the imposed and the measured displacement of three consecutive compressive cycles of the foam specimen.

For the first cycle, the path of the loading phase extends from 0 to $TI/2$ seconds, whereas the path of the unloading phase extends from $TI/2$ to $(TI - \theta)$ seconds. Thus, during the last θ seconds, the top plate loses contact with the foam specimen due to visco-elastic behavior of the material (Puri 2004). For the second and third cycles, the path of the loading phase extends from θ seconds to $(TI - \theta)$ seconds. Thus, the upper plate takes nearly the same delay (θ seconds) to regain contact with the material specimen. As shown in Fig. 4, there is a time lag between the zero positions of the measured displacement history and the imposed displacement. This time lag engenders a gap between the force–displacement curves of the first cycle and subsequent cycles, and it is graphically illustrated in Fig. 2 through the recovery regions. From the experimental point of view, this gap reflects the no data phase. In this study, we suggest to cure this gap by omitting the recovery regions as detailed in assumption (a) of Sect. 4.1.

According to Fig. 4, the expression of the measured displacement is deduced as:

$$x(t) = \begin{cases} \dot{x} \cdot t & 0 \leq t \leq \frac{T}{2}, \\ \dot{x} \cdot (T - t) & \frac{T}{2} \leq t \leq T. \end{cases} \quad (7)$$

Here $\dot{x} = 2A/T$ is the displacement rate, A the considered maximum displacement, and T the considered period of one cycle test.

3.2 Visco-elastic damping component

The hereditary model is the most appropriate approach to describe the pneumatic damping of foam during the loading half-cycle. Its formulations are drawn from the general differential consecutive law that relies on certain combinations of springs and dashpots (Ottosen and Ristinmaa 2005). In this modeling approach, the force, at a given time, is explicitly dependent on the integrated effect of previous displacement states, appropriately weighted by the relaxation kernel (Christensen 1982). Many authors including Yu and Haddad (1994) and Muravyov and Hutton (1997) assumed the kernel to be of exponential terms. Hence, the expression of the visco-elastic damping component is given by:

$$V_D(t) = \int_0^t \sum_{i=1}^N a_i e^{-\alpha_i(t-\tau)} \cdot \dot{x}(\tau) d\tau \quad (8)$$

where a_i and α_i are the visco-elastic parameters and N is the visco-elastic kernel order. The developed expression is deduced by the combination of Eqs. (7) and (8). Thus, we obtain the visco-elastic damping expression in displacement as follows:

$$V_D(x(t)) = \dot{x} \cdot \sum_{i=1}^N a_i \cdot \left(\frac{x(t)}{\dot{x} \cdot \alpha_i} - \frac{1}{\alpha_i^2} \cdot (1 - e^{-\alpha_i \cdot \frac{x(t)}{\dot{x}}}) \right). \quad (9)$$

3.3 Visco-elastic residual force component

Physically, the presence of the remaining strain after loading indicates that a residual force is created within the foam block, and it prevents the material from instantaneous full recovery. In fact, this residual force is generated by the quantity of energy stored in the material matrix during the loading half-cycles and released progressively after loading. Although this behavior resembles plasticity, it manifests the foam's visco-elastic properties that can be seen in static conditions, evidently its relaxation and creep behavior. However, during the recovery phase, the residual force decreases gradually over time and the material specimen regains its initial undeformed state. This behavior of recovery is physically more related to the phenomenon of relaxation rather than that of creep. For a multi-cycle test, the stored energy accumulates in microstructure elements of foam until it becomes full. Thus, in each cycle, a new residual force component is produced in the foam block but with lower magnitude compared with that of the previous cycle.

Mathematically, the fractional derivative approach is particularly favorable to model this visco-elastic effect because it has significant mathematical interpretations (Koeller 1984). Bagley and Torvik (1983) proposed a general form expressed as a sum of an elastic term and a fractional derivative term. In this work, we assume that the visco-elastic residual force component is an additive sum of only fractional derivative terms since the elastic term is

already contained in the elastic component. Thus, the expression of the residual force component is given as:

$$V_R(t) = \sum_{i=1}^M r_i \cdot D^{\beta_i} x(t) = \sum_{i=1}^M r_i \cdot \frac{d}{dt} \left[\frac{1}{\Gamma(1 - \beta_i)} \int_0^t (t - \tau)^{-\beta_i} \cdot x(\tau) d\tau \right]. \tag{10}$$

Here $\Gamma(x)$ is the complete gamma function; M is the order of the summation; β_i and r_i are respectively orders and coefficients of fractional derivative terms.

It can be observed that the fractional derivative operator (as used in Eq. (10)), may describe the memory effects of loading history since its mathematical formulation contains three needed tools to characterize the visco-elastic behavior: (i) the time derivative that specifies the changes of the material response over time, (ii) the convolution integral which signifies that the weight of residual effects in the present state depends on the location of previous disturbance in the time scale, and (iii) the fractional derivative order that involves an intermediate behavior between purely viscous and purely elastic properties. The developed expression is deduced by the combination of Eqs. (7) and (10). Therefore, we obtain the residual force expression in displacement as follows:

$$V_R(x(t)) = \sum_{i=1}^M \frac{2A \cdot r_i \cdot T^{-\beta}}{\Gamma(2 - \beta_i)} \cdot \left\{ \left(1 - \frac{x(t)}{2A} \right)^{(1-\beta_i)} - 2 \cdot \left(\frac{1}{2} - \frac{x(t)}{2A} \right)^{(1-\beta_i)} \right\}. \tag{11}$$

We note that mathematically both hereditary and fractional derivative approaches take a convolution form with different relaxation kernels since the hereditary model is derived from a differential equation with integer order while the fractional model is derived from the same constitutive law but with a non-integer order. This mathematical dissimilarity in relaxation kernels allows characterizing two different aspects of viscoelasticity in foam behavior: the viscoelastic damping effects and the viscoelastic residual effects. Thus, it appears that the hereditary approach is, through its exponential relaxation kernel, more appropriate to describe the short memory effects displayed on viscoelastic damping response of flexible polyurethane foam during loading phases, whereas the fractional derivative approach is, through its relaxation kernel, well suited to characterize the long memory and historical effects of the material especially during the unloading phases.

3.4 Elastic component

In the nonlinear elasticity literature, soft polyurethane foams have often been considered as rubber-like materials. This has stimulated many authors to use hyper-elastic models based on the use of the strain-energy function in the constitutive formulation to characterize nonlinear elasticity in flexible foam behavior. Among these models are the Ogden model (1972), the Yeoh model (1993), the Blatz–Ko model (1962), and many others. Yet, these models have generally been applied in numeric calculations and the finite element method. Pampolini and Del Piero (2008) proposed a model in which the open cell polyurethane foam is represented as a chain of elastic springs in order to identify the strain localization in the material. In this study, the nonlinear elastic component may well be expressed in terms of a polynomial function since it gives accurate results in the fitting process. Joshi et al. (2010) introduced a ninth order polynomial model to predict the nonlinear elastic stress in polyurethane foam response. In this modeling work, polynomial function with order P is

adopted to formulate the analytical expression of the nonlinear elastic component force as follows:

$$E(x(t)) = \sum_{i=0}^P k_i \cdot (x(t))^i. \quad (12)$$

Here k_i , $i = 0, \dots, P$, are the elastic stiffness parameters.

Indeed, the nonlinear elastic component of Eq. (12) is no more than a manifestation of the hyper-elastic response of foam in one dimension since its formulation allows describing the nonlinear elastic behavior of the material undergoing uniaxial large deformation reasonably well. Despite the fact that in energetic representations a single model allows representing various loading cases (Mills and Gilchrist 2000), these models do not actually account for visco-elastic effects. For this reason, the principle of modeling each effect apart is mainly adopted in this study.

4 Identification process

The cyclic force–displacement curves with the displacement cross-head speed of 23.6 mm/min are shown in Fig. 5. After setting to zero (as indicated in Figs. 4 and 5) the considered maximum displacement was 58 mm, and the test duration was 295 seconds.

4.1 Adopted assumptions for the identification method

In the present study, the identification process is based on three main assumptions:

- (a) The linear elastic and the recovery regions are omitted from the identification algorithm for many reasons. First, the linear elastic region is present only in the first loading half-cycle while it disappears in subsequent loading phases. Second, the recovery region (which indicates in itself the loss of contact between the material specimen and the top plate of the testing machine) is, by the same way, present in the first unloading half-cycle, while it fades from the second unloading phase. Third, the end of the linear elastic region of the first cycle corresponds, graphically, to the beginning of the subsequent cycles loading phase and at the same time to the beginning of recovery regions during the unloading half-cycles. This confirms that the nonlinear elastic component, already existing in both loading and unloading phases of the second and third cycles, does not exist in the linear elastic region of the first cycle.
- (b) The visco-elastic damping component depends only on the displacement rate and the maximum compression level. It is here not influenced by the number of cycles since we have the same displacement stroke in each loading phase (according to the first assumption and Fig. 5). Hence, the damping component is assumed to be the same in all loading half-cycles, and we have

$$V_{D1}(x(t)) = V_{D2}(x(t)) = V_{D3}(x(t)) = V_D(x(t)). \quad (13)$$

- (c) The nonlinear elastic component is dependent neither on the compression cross-head speed nor the number of cycles, and it has no hysteretic effects during unloading half-cycles. Thus, this component is the same whatever the testing phase, and we have

$$E_{L1}(x(t)) = E_{U3}(x(t)) = E(x(t)). \quad (14)$$

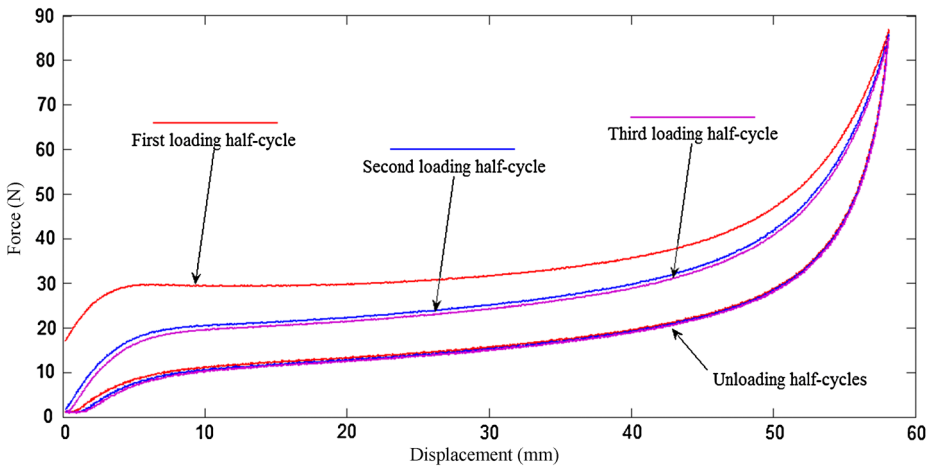


Fig. 5 Experimental data for a three-cycle uniaxial compressive test with the loading cross-head speed of 23.2 mm/min (curves are settled to zero after the elimination of the linear elastic and recovery regions)

The third assumption allows removing the elastic effects E by subtracting the response of the second loading half-cycle from that of the first unloading half-cycle. Then, we obtain the measurement data of the damping component force as follows:

$$V_D(x(t)) = F_{L2}(x(t)) - F_{U1}(x(t)). \tag{15}$$

The second hypothesis helps to remove the damping effects V_D by subtracting the response of the second loading half-cycle from that of the first loading half-cycle. This allows determining the measurement data of the visco-elastic residual force component of the first unloading phase V_{R1} as follows:

$$V_{R1}(x(t)) = F_{L2}(x(t)) - F_{L1}(x(t)). \tag{16}$$

The second and the third visco-elastic residual force components are calculated by establishing the difference force respectively between the second and the first and the third and the second unloading phases. Thus, the expressions of these components are given as:

$$V_{R2}(x(t)) = F_{U2}(x(t)) - F_{U1}(x(t)), \tag{17}$$

$$V_{R3}(x(t)) = F_{U3}(x(t)) - F_{U2}(x(t)). \tag{18}$$

Respecting the nonlinear elastic component force, it can be deduced by establishing the difference between the response of the first loading half cycle and the damping component measurement data as follows:

$$E(x(t)) = F_{L1}(x(t)) - V_D(x(t)). \tag{19}$$

Therefore, the rheological equations giving the expressions of the total force exerted by the foam sample and its components during the six half-cycles are assumed to be:

$$F_{L1}(x(t)) = E(x(t)) + V_D(x(t)), \quad (20a)$$

$$F_{U1}(x(t)) = E(x(t)) + V_{R1}(x(t)), \quad (20b)$$

$$F_{L2}(x(t)) = E(x(t)) + V_D(x(t)) + V_{R1}(x(t)), \quad (20c)$$

$$F_{U2}(x(t)) = E(x(t)) + V_{R1}(x(t)) + V_{R2}(x(t)), \quad (20d)$$

$$F_{L3}(x(t)) = E(x(t)) + V_D(x(t)) + V_{R1}(x(t)) + V_{R2}(x(t)), \quad (20e)$$

$$F_{U3}(x(t)) = E(x(t)) + V_{R1}(x(t)) + V_{R2}(x(t)) + V_{R3}(x(t)). \quad (20f)$$

The subsequent stage contains a validation of the model formulation by simulating the total foam force of the three consecutive cycles.

4.2 Optimization algorithm and methods

The flowchart of the parameter identification process is described in Fig. 6. In each stage, the optimization system of parameters consists of the fitting of the mathematical model with measurement data. Numeric calculations involve minimizing a cost function which represents the least mean square error between measurement data and analytical formulations of the model. These numeric calculations were executed in *Matlab*, by exploiting the optimization toolbox and the curve fitting toolbox. The '*lsqnonlin*' function provides two deterministic methods to find minimums of nonlinear least squares problems: Trust region reflective and Levenberg–Marquardt. Both methods were used to estimate the model parameters. Curve fitting toolbox was also exploited to predict the stiffness parameters of the elastic component force as well as giving the starting point values. The major advantage of the identification methodology, presented in the flowchart of Fig. 7, is that it helps to extract the measurement data of each component force one by one, and then to calibrate its parameters separately. This advantage allows avoiding the admixture problem that occurs often in the difference force method, and that requires selecting among the found minimums the one which gives a physical meaning and verifies the thermodynamic consistency. In the case of this study, the deterministic methods are well suited to solve the optimization problems, since we have a known prior shape of the curve of each component force. Furthermore, these methods take relatively short calculation time compared with random methods (e.g., genetic algorithm, Monte Carlo, and Nelder–Mead algorithm). In general, the calculation time depends on both the initial guess (provided by the curve fitting toolbox) and the stopping criterion (which was set as 10^{-20} in our cases).

4.3 Thermodynamic consistency of the model parameters

The thermodynamic consistency requires that the established model give simulations that satisfy causality and stability conditions. This implies that the dissipated energy in deforming the foam block should be non-negative. According to the approach proposed by Bagley and Torvik (1986), the real and imaginary parts of the frequency response of the linear part of the model (Deng et al. 2004) must be non-negative. For the first cycle, the respective Fourier transforms $G_{L1}(j\omega)$ and $G_{U2}(j\omega)$ of the linear parts of the pulse model responses of the loading and the unloading phases are:

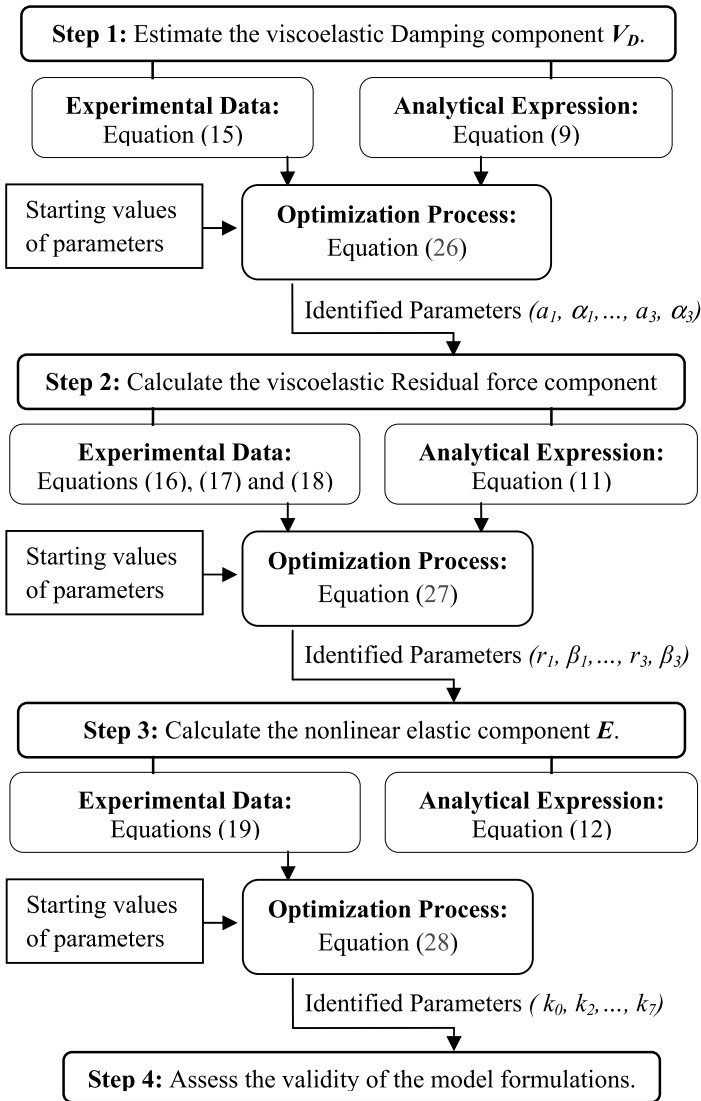


Fig. 6 Algorithm of the parameter identification process

$$G_{L1}(j\omega) = k_1 + \sum_{n=1}^3 \frac{a_n}{j\omega - \alpha_n}, \tag{21}$$

$$G_{U1}(j\omega) = k_1 + \sum_{m=1}^3 r_m(j\omega)^{\beta_m}. \tag{22}$$

As indicated above, the causality and stability conditions involve that the real and imaginary parts of $G_{L1}(j\omega)$ and $G_{U2}(j\omega)$ must be positive. As the material is compressed in quasi-static regime and then with low frequency, the thermodynamic constraints of the

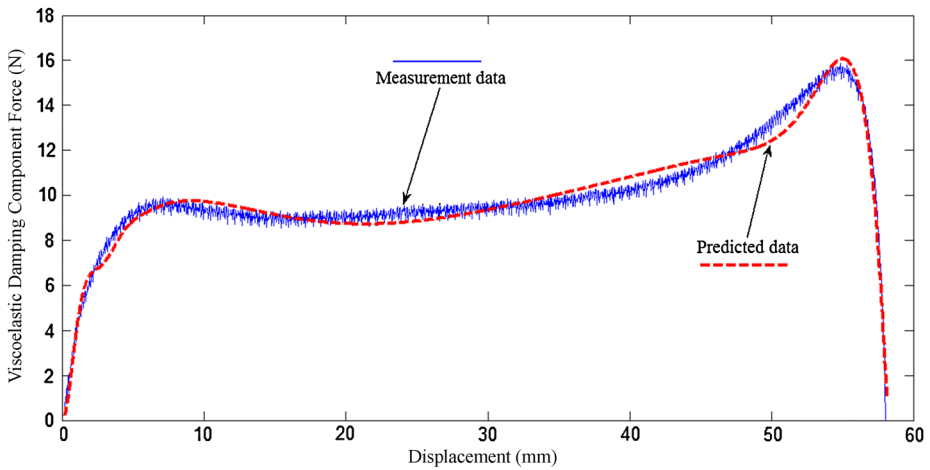


Fig. 7 Experimental data and estimated visco-elastic damping force

model parameters can be obtained by limiting the study to the case of $\omega \rightarrow 0$. Therefore, in the case of low frequency, we obtain the following thermodynamic constraints of the model parameters:

$$k_1 - \frac{a_1 \cdot \text{Re}(\alpha_1)}{\alpha_1 \bar{\alpha}_1} - \frac{a_2 \cdot \text{Re}(\alpha_2)}{\alpha_2 \bar{\alpha}_2} - \frac{a_3 \cdot \text{Re}(\alpha_3)}{\alpha_3 \bar{\alpha}_3} \geq 0 \tag{23}$$

$$\frac{a_1 \cdot \text{Im}(\alpha_1)}{\alpha_1 \bar{\alpha}_1} + \frac{a_2 \cdot \text{Im}(\alpha_2)}{\alpha_2 \bar{\alpha}_2} + \frac{a_3 \cdot \text{Im}(\alpha_3)}{\alpha_3 \bar{\alpha}_3} \geq 0 \tag{24}$$

$$k_1 \geq 0 \tag{25}$$

We should note that exactly the same equations could be found if the cases of the second or the third cycles were addressed. Finally, the mathematical constraints of Eqs. (23), (24), and (25) should be proven by the obtained parameters to ensure that the proposed model meets the thermodynamic constancy.

4.4 Prediction of the visco-elastic damping component

In this step, removing elastic and residual effects from the second loading response results in an expression depending only on the damping parameters. The measurement data is acquired by subtracting the first unloading response from the second total loading force at the same compression level.

Equations (9) and (15) were utilized in the optimization algorithm. The visco-elastic damping parameters are identified by minimizing the cost function Q_1 expressed as

$$Q_1(a_1, \alpha_1, \dots, a_N, \alpha_N) = \sum_{i=1}^S (V_{D_{\text{data}}}(i \cdot \delta x) - V_D(i \cdot \delta x))^2. \tag{26}$$

Here S is the sampling number ($A = S \cdot \delta x$). The measurement and the predicted data of the visco-elastic damping force are plotted in Fig. 7.

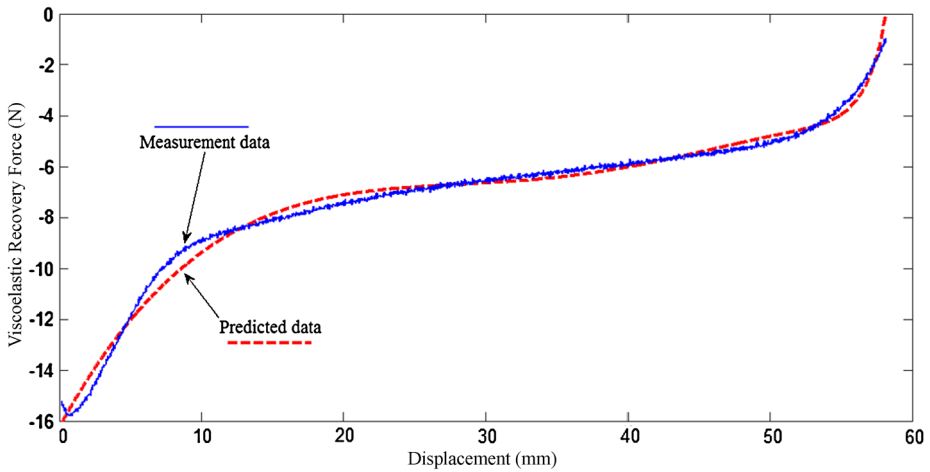


Fig. 8 Measurement and predicted data of the visco-elastic residual force of the first unloading half-cycle

The values of optimized parameters are contained in Table 2. It is found that a good simulation is obtained by the third order hereditary model. The fitting results of the second order model were not satisfactory. In fact, the model prediction accuracy is obtained by considering the parameters a_1 , a_2 , and a_3 to be real, while the parameters α_1 , α_2 , and α_3 chosen to be complex.

4.5 Prediction of the visco-elastic residual force component

The visco-elastic residual force component data is calculated by using Eqs. (16), (17) and (18). The analytical formulation is given by Eq. (11). The visco-elastic residual force parameters are identified by minimizing the cost function Q_{II} expressed as

$$Q_{II}(R_1, \beta_1, \dots, R_L, \beta_L) = \sum_{i=1}^S (V_{R_{data}}(i \cdot \delta x) - V_R(i \cdot \delta x))^2. \tag{27}$$

The measurement and the predicted data of the visco-elastic residual force are illustrated in Figs. 8 and 9.

The values of optimized parameters are grouped in Table 3. It is found that the third order fractional derivative model provides acceptable simulations while the second order model did not produce accurate calibration results.

4.6 Prediction of the nonlinear elastic component

Estimation calculations were executed by minimizing the cost function Q_{III} expressed as

$$Q_{III}(k_1, \dots, k_7) = \sum_{i=1}^S (E_{data}(i \cdot \delta x) - E(i \cdot \delta x))^2. \tag{28}$$

E_{data} is the reference data of the elastic component generated from Eq. (19), and E is the analytical expression given by Eq. (12). The plots of the measurement and the estimated data of the nonlinear elastic force are shown in Fig. 10.

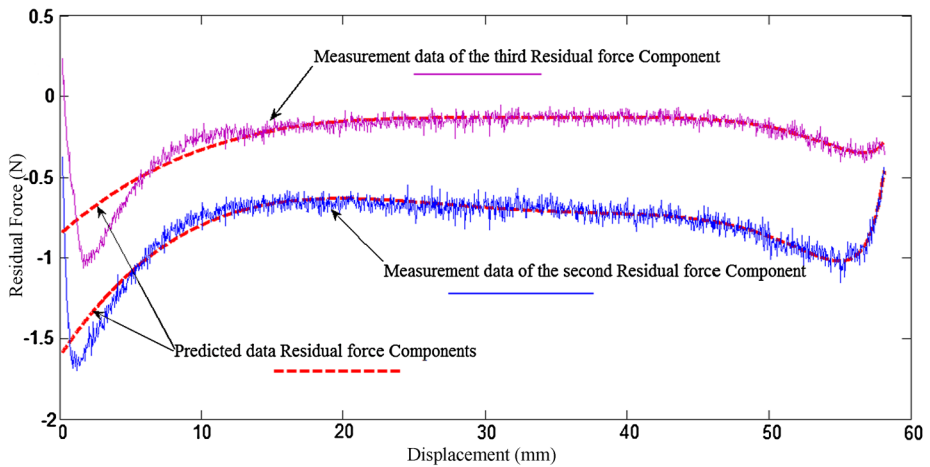


Fig. 9 Measurement and predicted data of the visco-elastic residual force of the second and third unloading half-cycles

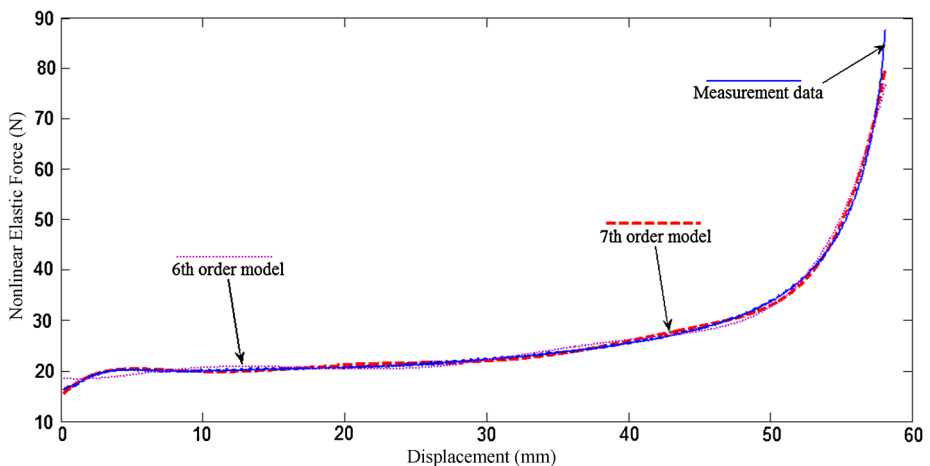


Fig. 10 Elastic component data and calibrated curves with different polynomials orders

Parameter optimization is performed by exploiting the “*lsqcurvefit*” tool of Matlab. We mention here that different polynomial orders were considered in the optimization process. As shown in Fig. 10, it is found that the polynomial model with order $P = 7$ yields an optimal simulation. The estimated stiffness parameters are illustrated in Table 4.

5 Validation results and discussion

The following Tables 2–4 show the resulting values of the model identified parameters.

In Fig. 11, we show the experimental data and the predicted results of total foam response under a cyclic uniaxial compressive test. From Tables 2 and 4, it is clear that the

Table 2 Values of estimated damping parameters

Parameters	Units	Values
a_1	(N m s ⁻¹)	-2.656×10^{-12}
a_2	(N m s ⁻¹)	-0.207
a_3	(N m s ⁻¹)	5.576
Re(α_1)	(s ⁻¹)	-0.192
Im(α_1)	(s ⁻¹)	0.177
Re(α_2)	(s ⁻¹)	0.055
Im(α_2)	(s ⁻¹)	0.046
Re(α_3)	(s ⁻¹)	0.319
Im(α_3)	(s ⁻¹)	0.810

Table 3 Values of estimated residual force parameters

Parameters	Units	First cycle	Second cycle	Third cycle
r_1	(N s ^{β_1} m ⁻¹)	2876.676	522.936	229.6489
r_2	(N s ^{β_2} m ⁻¹)	7.962	1.306	0.6214
r_3	(N s ^{β_3} m ⁻¹)	8.624×10^{-4}	1.106×10^{-4}	6.264×10^{-5}
β_1	-	0.9926	0.9917	0.9939
β_2	-	-0.1528	-0.1774	-0.1585
β_3	-	-1.9594	-2.0282	-1.9771

Table 4 Values of estimated elastic stiffness parameters

Parameters	Units	Values
k_0	(N)	14.910
k_1	(N m ⁻¹)	2.987
k_2	(N m ⁻²)	-0.598
k_3	(N m ⁻³)	0.0557
k_4	(N m ⁻⁴)	-0.0027
k_5	(N m ⁻⁵)	7.0733×10^{-5}
k_6	(N m ⁻⁶)	-9.410×10^{-7}
k_7	(N m ⁻⁷)	5.0053×10^{-9}

thermodynamic conditions of Eqs. (23), (24), and (25) are verified by the parameter values.

However, the approach of Sect. 4.3 conduces to mathematical constraints that do not include all parameters. For further discussion of the model results validity, we propose examining three efficiency requirements: (i) accuracy of predicted simulations with experimental data, (ii) capacity to reproduce visco-elastic phenomena engendered in the response of flexible polyurethane foam undergoing a cyclic uniaxial compressive test, and (iii) physical significance of results and accordance with the phenomenological identification of the force–displacement curve.

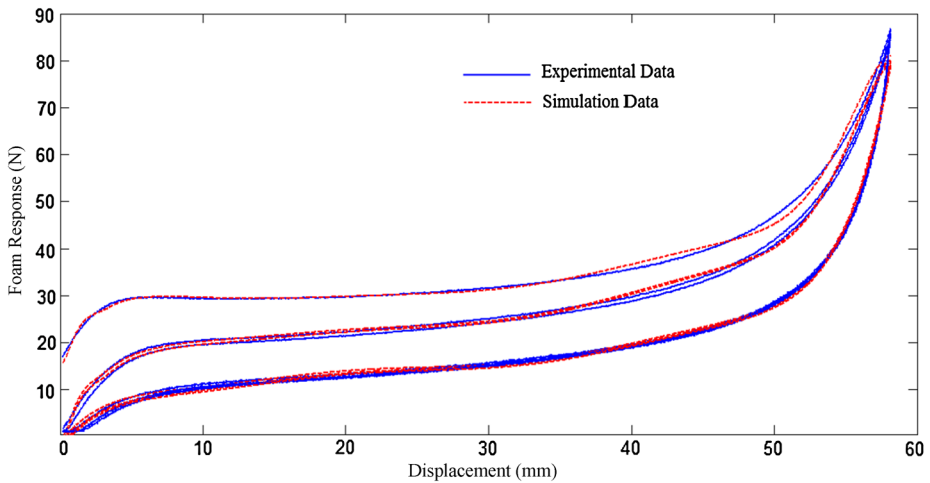


Fig. 11 Experimental and predicted total response of foam

Table 5 Fit statistics

Optimization process	SSE	R-square	Adj. R-square	RMSE
Step 1	326.204	0.958	0.9553	0.4758
Step 2	127.754	0.9886	0.9884	0.2975
Step 3	657.685	0.996	0.996	0.6754

5.1 Accuracy of the model fit

As shown in Figs. 7–10, it is clear that the model formulations and the optimization process lead to accurate simulation results with little bias. The fit statistics relative to each identification algorithm step are illustrated in Table 5.

As shown in Table 5, we note that the R-square values of the optimization process steps are very close to 1. This indicates that the major proportions of variance of each of the three measurement data are considered by the model. Moreover, the adjusted R-square values affirm that prediction results have good quality, since fits explain at least 95 % of the total variation in experimental data about the average values. From Fig. 11, it should be mentioned that the bound point between the loading and the unloading phases is slightly shifted in the simulated curves. This is due to a weak failure at this point induced from the identification process of the elastic component as it appears in Fig. 10. In fact, this does not affect the global simulated response as it takes a local point. To sum up, the model simulations of the three cycles display good accuracy.

5.2 Capacity of reproducing visco-elastic phenomena

The major important manifestation of soft foam visco-elastic behavior during multi-cycle tests is the drop in the material reacting force between the first and the second cycle; however, this change recurs slightly from the second to third cycle (Rehkopf et al. 1994). This phenomenon is perfectly reproduced by the model as visco-elastic residual effects are accounted for by its formulations. Moreover, the identification process allows calibrating the

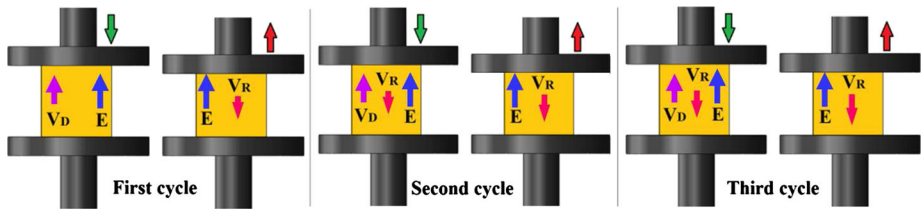


Fig. 12 Schematic representation of overall foam response components directions

magnitude of the residual force in each testing phase. Modeling this component force makes it possible to understand and characterize another visco-elastic manifestation which is the remaining strain effects when the loading force is removed. Concerning the hysteretic effect, it is explained by the damping component force that considers the two mechanisms of energy dissipation in flexible foams: the flow of the air in the material cells and the friction within the cellular matrix.

5.3 Physical significance of results

For modeling purposes, analytical formulations were founded on the phenomenological force–displacement curve identification (explained in the first section). Agreement between prediction results and the hypothesis of the phenomenological curve identification is a strong indicator of the model validity.

Concerning the residual force components, it can be clearly seen in Fig. 9 that the second and the third residual force components curves have identical shapes and close magnitudes. This repeatability affirms the good agreement between experiments and model formulations. In addition, the difference of magnitude between the first residual force component and subsequent components is a visco-elastic manifestation that we seek to characterize. Moreover, it can be observed from Figs. 7–9 that the residual force component force has a relatively low magnitude compared to damping and elastic components. This result is reasonable and in good agreement with phenomenological assumptions as the elastic component is strongly dominant during the unloading phase in soft foam response. Otherwise, the magnitude of the first residual force is very faithful to experimental observations since the material restores immediately up to 96 % of its initial height. Yet, the remaining strain corresponds to the length of recovery region. The residual force can also be graphically determined by finding the force in the linear elastic region corresponding to the beginning of the second cycle. Moreover, it was shown in Figs. 8 and 9 that residual forces have negative values. This indicates that residual forces are opposed to elastic force during unloading phases. From an experimental viewpoint, this opposition can be explained likewise by the existence of remaining strain effects just after each unloading half-cycle. Hence, the visco-elastic residual force is the physical origin of the loading history dependence of polyurethane foam. In Fig. 12, we illustrate a schematic representation accounting for the directions of existing forces in overall foam response during compression and decompression half-cycles.

Therefore, the memory effects in soft polyurethane foams correspond to the visco-elastic nature of the polymer matrix and its capacity to store energy during the loading phase and to liberate this energy logarithmically when the material is completely unloaded.

If we address the changes of the residual force parameters with the number of cycles, we can clearly see that parameters r_1 , r_2 , and r_3 decrease from the first to the second cycle and afterwards from the second to the third cycle. This decrease in values of these parameters

may be attributed to the stress softening behavior in flexible polyurethane foam caused by repetitive loading. However, the values of parameters β_1 , β_2 , and β_3 decrease slightly from the first to the second cycle, and increase again a bit from second to third cycle. These small fluctuations (around 0.2 % for parameter β_1 , 10 % for parameter β_2 , and 3 % for parameter β_3) indicate that the parameter β_i can be considered almost independent of the number of cycles.

Respecting the damping force curve, it can be clearly seen from Fig. 7 that three regions can be distinguished: region of the first peak, plateau region, and region of the second peak. The first region indicates that the air within the material microstructure is still motionless, and visco-elasticity is exhibited by the polymer matrix response. It can be considered as the yield point since it comes next to linear zone. In the plateau region, the damping force is governed by the air flow rate through the polymer matrix and the polyurethane foam structure (closed cell or open cell). At the second peak, the foam sample is compacted; it manifests as a rubber-like solid.

6 Conclusion

A combined model with two visco-elastic components and an elastic component was established to predict a multi-cycle behavior of soft polyurethane foam undergoing quasi-static uniaxial compressive tests. The elastic component was modeled as a seventh order polynomial function. The visco-elastic components were modeled with two different approaches: the hereditary approach was used to formulate visco-elastic damping component, while the fractional derivative approach was utilized to formulate the visco-elastic residual force component. A parameter optimization process based on the isolation of each component measurement data was developed to calibrate its parameters. This identification methodology helps to avoid the admixture problem which occurs in the difference force method. The obtained results were accurate when compared with experiments, and the estimated component forces have reasonable physical significances and were in agreement with new force–displacement curve identification presented in the first section. However, a generalization of this model requires checking its ability to cover a wide range of loading rates in a quasi-static regime.

References

- Bagley, R.L., Torvik, P.J.: A theoretical basis for the application of fractional calculus to viscoelasticity. *J. Rheol.* **27**(3), 201–210 (1983)
- Bagley, R.L., Torvik, P.J.: On the fractional calculus model of viscoelastic behavior. *J. Rheol.* **30**(1), 133–155 (1986)
- Blatz, P.J., Ko, W.L.: Application of finite elastic theory to the deformation of rubbery materials. *Trans. Soc. Rheol.* **6**, 223–251 (1962)
- Christensen, R.: *Theory of Viscoelasticity*. Academic Press, New York (1982)
- Del Piero, G., Pampolini, G.: The influence of viscosity on the response of open-cell polymeric foams in uniaxial compression: Experiments and theoretical model. *Contin. Mech. Thermodyn.* **24**(3), 181–199 (2012)
- Deng, R., Davies, P., Bajaj, A.K.: A case study on the use of fractional derivatives: the low-frequency viscoelastic unidirectional behavior of polyurethane foam. *Nonlinear Dyn.* **38**, 247–265 (2004)
- Deng, R., Davies, P., Bajaj, A.K.: A nonlinear fractional derivative model for large uniaxial deformation behavior of polyurethane foam. *Signal Process.* **86**, 2728–2743 (2006)
- Ferry, J.D.: *Viscoelastic Properties of Polymers*. Wiley, New Jersey (1970)
- Gauch, H.G. Jr.: Winning the accuracy game. *Am. Sci.* **94**, 133–141 (2006)

- Gibson, L.J., Ashby, M.F.: *Cellular Solids: Structure and Properties*, 2nd edn. Cambridge University Press, Cambridge (1997)
- Ippili, R.K., Widdle, R.D., Davies, P., Bajaj, A.K.: Modeling and identification of polyurethane foam in uniaxial compression: combined elastic and viscoelastic response. In: *Proceedings of the 2003 ASME Design Engineering Technical Conferences, DETC2003/VIB-48485*, Chicago, Illinois, pp. 2–6 (2003)
- Jmal, H., Dupuis, R., Aubry, E.: Quasi-static behavior identification of polyurethane foam using a memory integer model and the difference-forces method. *J. Cell. Plast.* **47**(5), 447–465 (2011)
- Joshi, G., Anil, K., Bajaj, A.K., Davies, P.: Whole-body vibratory response study using a nonlinear multi-body model of seat-occupant system with viscoelastic flexible polyurethane foam. *Ind. Health* **48**, 663–674 (2010)
- Koeller, R.C.: Applications of fractional calculus to the theory of viscoelasticity. *J. Appl. Mech.* **51**, 299–307 (1984)
- Mills, N.J., Gilchrist, A.: Modelling the indentation of low density polymer foams. *Cell. Polym.* **19**(6), 389–412 (2000)
- Muravyov, A., Hutton, S.G.: Closed-form solutions and the eigenvalue problem for vibration of discrete viscoelastic systems. *J. Appl. Mech.* **64**, 684–691 (1997)
- Nutting, P.G.: A new general law of deformation. *J. Franklin Inst.* **191**, 679–685 (1921)
- Ogden, R.W.: Large deformation isotropic elasticity: on the correlation of theory and experiment for compressible rubber like solids. *Proc. R. Soc. A, Math. Phys. Eng. Sci.* **328**, 567–583 (1972). 1575
- Ottosen, N.S., Ristinmaa, M.: *The Mechanics of Constitutive Modeling*. Elsevier, Amsterdam (2005)
- Pampolini, G., Del Piero, G.: Strain localization in open-cell polyurethane foams: experiments and theoretical model. *J. Mech. Mater. Struct.* **3**(5), 969–981 (2008)
- Puri, T.: Integration of polyurethane foam and seat occupant models to predict the settling point of a seat occupant. Master's thesis, Purdue University, School of Mechanical Engineering, West Lafayette, IN 47907 (2004)
- Rehkopf, J.D., McNeice, G.M., Brodland, G.W., Kuczynski, E.T., Kerman, M.: Dynamic behavior of an automotive polyurethane foam under multiple compression cycles. SAE 940876 (1994)
- Rouse, P.E. Jr.: A theory of the linear viscoelastic properties of dilute solutions of coiling polymers. *J. Chem. Phys.* **21**(7), 1272–1280 (1953)
- Singh, R.: Dynamic modeling of polyurethane foam and development of system identification methodologies. Master's Thesis, School of Mechanical Engineering, Purdue University, West Lafayette, IN 47907 (2000)
- White, S.W., Kim, S.K., Bajaj, A.K., Davies, P., Showers, D.K., Liedtke, P.E.: Experimental techniques and identification of nonlinear and viscoelastic properties of flexible polyurethane foam. *Nonlinear Dyn.* **22**, 281–313 (2000)
- Yeoh, O.H.: Some forms of the strain energy function for rubber. *Rubber Chem. Technol.* **66**, 754–771 (1993)
- Yu, P., Haddad, Y.M.: A dynamic system identification method for the characterization of the rheological response of a class behavior of viscoelastic materials. *Int. J. Press. Vessels Piping* **61**, 87–97 (1994)